JACS
JOURNAL OF THE AMERICAN CHEMICAL SOCIETY
pubs.acs.org/JACS
Article

Two-State Reactivity in Iron-Catalyzed Alkene Isomerization Confers σ-Base Resistance

Sean A. Lutz,[†] Anne K. Hickey,[†] Yafei Gao,[†] Chun-Hsing Chen, and Jeremy M. Smith*

Cite This: J. Am. Chem. Soc. 2020, 142, 15527−15535
Read Online
ACCESS | Metrics & More | Article Recommendations | Supporting Information

ABSTRACT: A low-coordinate, high spin (S = 3/2) organometallic iron(I) complex is a catalyst for the isomerization of alkenes. A combination of experimental and computational mechanistic studies supports a mechanism in which alkene isomerization occurs by the allyl mechanism. Importantly, while substrate binding occurs on the S = 3/2 surface, oxidative addition to an η^1-allyl intermediate only occurs on the S = 1/2 surface. Since this spin state change is only possible when the alkene substrate is bound, the catalyst has high immunity to typical σ-base poisons due to the antibonding interactions of the high spin state.

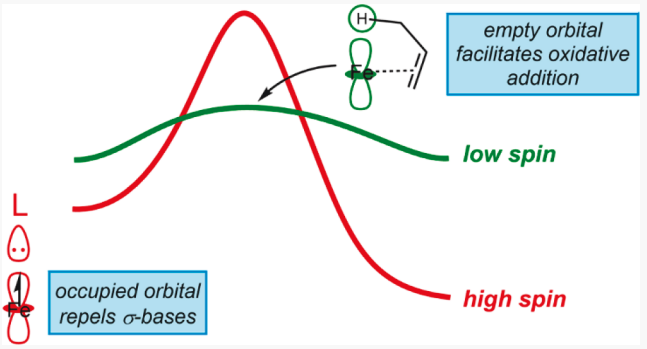

INTRODUCTION

Driven in part by perceived advantages in cost and toxicity, recent years have seen an explosion of interest in the development of iron-based catalysts for transformations of organic substrates.[1,2] While substantial efforts have been made toward developing iron catalysts that replicate the reactivity of noble metal congeners, it has also been recognized that new catalysts may benefit from the intrinsic properties of iron.[3] Most notably, the rich landscape of redox and spin states associated with iron complexes has the potential for accessing reactivity that is largely unavailable to noble metal complexes.

Due to relatively small ligand field strengths, particularly with low coordination numbers, iron complexes are often high spin; moreover the changes in geometry, ligands, and/or oxidation state that occur during the course of a reaction may also be associated with changes in the metal spin state. "Two-state reactivity" emerges when these spin state changes lower the energy of the transition state (Figure 1).[4] While extensively investigated in the context of high valent iron oxo chemistry,[5] two-state reactivity has also been proposed for low valent organometallic iron complexes, with the prototypical example being the transient 16-electron species $^3Fe(CO)_4$.[6] Although this species has a triplet ground state, reactions involving ligand binding require spin crossover to the low-lying $^1Fe(CO)_4$ state.[7]

Two-state reactivity has been proposed for the reactions of a number of low-coordinate iron complexes, including β-hydride elimination from three-coordinate Fe(II) alkyl complexes,[8] oxidative addition by four-coordinate Fe(0) complexes[9] and C−H activation by Fe(II) complexes.[10] Moreover, multiple spin states have been implicated in the reaction mechanisms of low valent iron catalysts,[11] including aldehyde hydrosilylation,[12]

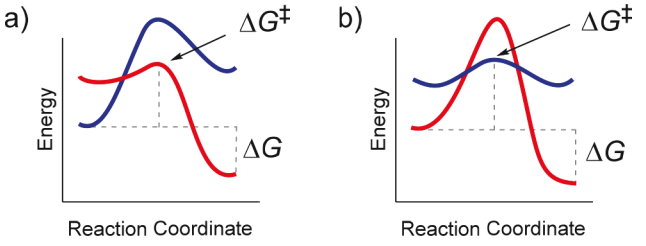

Figure 1. Reaction coordinates for two-state reactivity leading to lowered activation barriers. Red and blue curves represent different spin states. (a) Spin state change occurs before the transition state, providing a product with a different spin state than reactant; (b) transition state is on a different spin state than reactant and product, leading to "spin acceleration".

alkene-isomerization-hydroboration,[13] [2 + 2] cycloadditions,[14] and C−C coupling.[15]

Due to differential occupancies of antibonding orbitals, simple ligand field considerations lead to the expectation that two spin states of the same d-electron count may differ in their reactivity. Indeed, it has been shown that both the redox potentials and activation energies for electron transfer in a series of cytochrome P450 substrate analogues are directly related to the spin state of iron(III).[16,17] We hypothesized that such spin-state reactivity

Received: July 7, 2020
Published: August 12, 2020

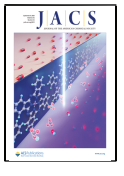

https://dx.doi.org/10.1021/jacs.0c07300
J. Am. Chem. Soc. 2020, 142, 15527−15535

Scheme 1

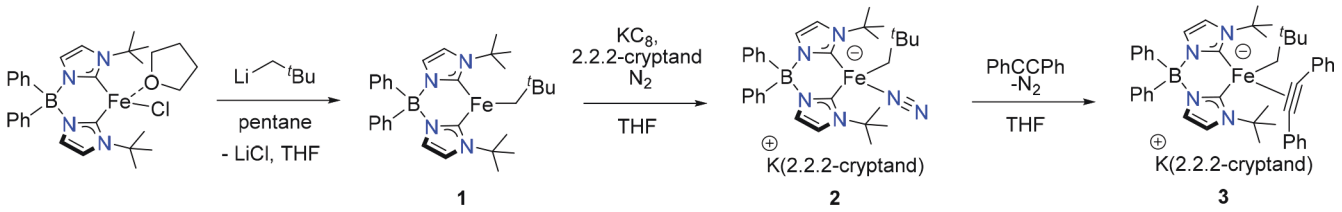

differences could be used to engineer catalyst selectivity. Specifically, we anticipated that entry into the catalytic cycle could be gated by substrates that convert the catalyst spin state to that of the transition state for an appropriate elementary step. For example, substrates that convert a high spin catalyst to its low spin form are expected to create the appropriate d-orbital vacancies required for $2e^-$ organometallic reactions.

In this work, we report a high spin ($S = 3/2$) iron(I) complex that is a catalyst for a model organometallic reaction, namely alkene isomerization. A combined experimental and computational investigation reveals the involvement of two spin states, with the transition states for substrate isomerization only accessible on the low spin ($S = 1/2$) surface. Since the partially filled d-orbitals of the high spin state result in weak ligand binding in the ground state, this confers immunity against typical σ-basic catalyst poisons. To the best of our knowledge, this work shows for the first time that the attributes of two-state reactivity allow for new reaction selectivity. We anticipate that the concepts described for this model system will be applicable to other catalytic reactions.

RESULTS AND DISCUSSION

Synthesis and Characterization. Treatment of the iron chloride precursor $Ph_2B(^tBuIm)_2FeCl(THF)$[18] with 1 equiv of $LiCH_2{}^tBu$ in pentane gives the yellow complex $Ph_2B(^tBuIm)_2FeCH_2{}^tBu$ (**1**) in 95% yield (Scheme 1). The molecular structure of **1** shows a planar, three-coordinate iron center, with the sum of angles about iron = 359.9° (Figure 2). The iron-carbene bond distances of 2.1000(13) and 2.0936(14) Å are consistent with a high spin ($S = 2$) configuration. The distance to the α carbon of the neopentyl ligand is 2.0534(15) Å, similar to previously characterized high spin iron(II) alkyl complexes.[19] At 80 K, the ^{57}Fe Mössbauer spectrum of **1** shows a symmetric quadrupole doublet centered at $\delta = 0.34$ mm/s, with $\Delta E_Q = 1.41$ mm/s, similar to three-coordinate high-spin iron(II) β-diketiminate[20] and iron(II) NHC alkyl complexes.[21] The solution magnetic moment, determined by Evans' method ($\mu_{eff} = 5.0(3)\ \mu_B$), confirms the high spin formulation of complex **1**.

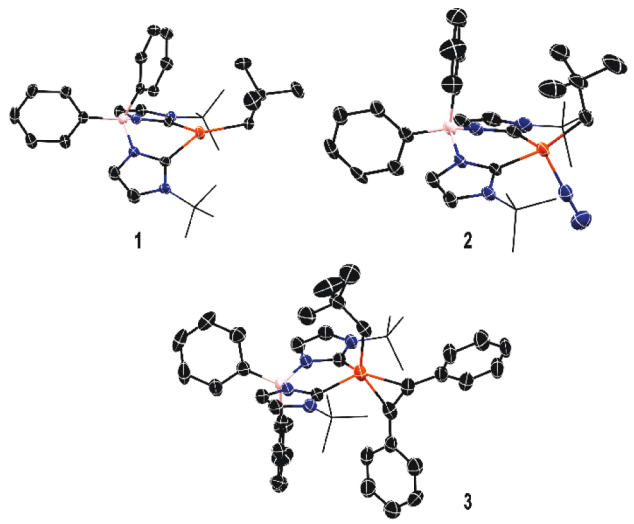

Figure 2. Molecular structures of **1**−**3**. Thermal ellipsoids are shown at 50% probability, ligand *tert*-butyl groups represented as wireframes, and hydrogen atoms and the $[K(2.2.2\text{-cryptand})]^+$ cation of **2** and **3** omitted for clarity. Pink, black, orange, and blue ellipsoids represent boron, carbon, iron, and nitrogen atoms, respectively.

Reducing **1** by 1 equiv of KC_8 in the presence of 2.2.2-cryptand provides dark red $[K(2.2.2\text{-cryptand})][Ph_2B(^tBuIm)_2FeCH_2{}^tBu(N_2)]$ (**2**) in 60% yield following workup. The molecular structure of **2** shows a four-coordinate iron center, with the bis(carbene)borate, neopentyl and dinitrogen ligands completing the coordination sphere (Figure 2). The iron-carbene (2.117(4) and 2.113(4) Å) and iron-neopentyl (2.121(5) Å) bond distances are longer than in **1**, suggesting that iron remains high spin after reduction.[22]

While no resonances are observed between +200 and −60 ppm in the ^{1}H NMR spectrum of **2**, a strong N−N stretch at 1897 cm^{-1} confirms that the N_2 ligand remains bound to iron. This frequency is significantly lower than other four-coordinate iron(I) complexes such as $[Li(Et_2O)_2][^{iPr}PDIFe(CH_2{}^tBu)(N_2)]$ (ν_{NN} = 1948 cm^{-1}), (PNP)Fe(N_2) (PNP = 2,5-bis(di-*tert*-butylphosphinomethyl)pyrrolide) (1964 cm^{-1}), $[(ICy)_3Fe(N_2)][BPh_4]$ (ICy = 1,3-dicyclohexylimidazol-2-ylidene) (1967 cm^{-1}), or $PhB(AdIm)_3FeN_2$ (1928 cm^{-1})[23] suggesting a high degree of π-backbonding in **2**. A doublet centered at $\delta = 0.52$ mm/s ($\Delta E_Q = 1.70$ mm/s) is observed in the Mössbauer spectrum of **2** (80 K), whose asymmetry is likely due to the onset of slow relaxation in this noninteger spin complex.[24] While the differences in coordination geometry between **1** and **2** hinder direct comparison of the spectroscopic parameters, the greater isomer shift in **2** relative to **1** is consistent with a high spin iron(I) assignment.[23c,25] In addition, these parameters are comparable to high-spin iron(I) hydride complexes supported by a β-diketiminate ligand.[26] Complex **2** is therefore assigned as high-spin ($S = 3/2$) iron(I), which is also consistent with the solution magnetic moment ($\mu_{eff} = 4.2(3)\ \mu_B$).

Complex **2** reacts with one equivalent of PhC≡CPh to yield purple $[K(2.2.2\text{-cryptand})][Ph_2B(^tBuIm)_2Fe(CH_2{}^tBu)(\eta^2\text{-PhC}{\equiv}\text{CPh})]$ (**3**) in 65% isolated yield. The molecular structure of **3** confirms the formulation of the product, with η^2−PhC≡CPh replacing the dinitrogen ligand (Figure 2). The Fe−C bond to the neopentyl ligand is nearly parallel with the acetylene ligand (torsion angle 166.6(4)°) and is almost perpendicular to the C−Fe−C plane containing the donor atoms of the bis(carbene)borate ligand (torsion angle 86.6(4)°). The C−C bond distance of 1.281(7) Å is elongated from free PhC≡CPh due to strong backdonation from the iron center.

https://dx.doi.org/10.1021/jacs.0c07300
J. Am. Chem. Soc. 2020, 142, 15527−15535

Unlike its precursor **2**, the ^{1}H NMR spectrum of complex **3** displays resonances between 35 and −10 ppm, although the spin state is unchanged (S = 3/2), as determined by Evans′ method (μ_{eff} = 5.1(3) μ_B). The C≡C stretching frequency presents at 1769 cm^{-1} (KBr), similar to C≡C stretches observed for acetylene adducts of iron(I) β-diketiminate complexes.[27] The ^{57}Fe Mössbauer spectrum of complex **3** at 80 K shows a symmetric doublet with an isomer shift δ = 0.42 mm/s and quadrupole splitting ΔE_Q = 1.99 mm/s. This isomer shift is lower than that of complex **2**, consistent with a greater degree of π-backbonding from iron into better π-acid diphenylacetylene. The increased backbonding increases the covalency between the ligand and metal, which in turn decreases the isomer shift.[28]

Catalytic Alkene Isomerization. Complex **2** catalyzes the isomerization of 1-hexene to 2-hexene (10 mol % **2**, 40 °C). Complete isomerization to 2-hexene in a 4:1 trans:cis ratio occurs within 24 h, as determined by ^{1}H and ^{13}C{^{1}H} NMR spectroscopies.[29] This ratio is that expected based on the thermodynamic stabilities of the two isomers, suggesting there is no kinetic selectivity. While we have not attempted to optimize the catalytic conditions, the mild reaction conditions are notable. By contrast, the iron(II) complex **1** does not catalyze 1-hexene isomerization.

Since iron nanoparticles have been previously implicated in the catalytic isomerization of alkenes,[30] we have conducted control experiments to test for nanoparticle formation. While the limited solubility of elemental iron in mercury[31] is a complicating factor, it is notable that the addition of elemental mercury does not impede the catalytic activity of **2**. Additionally, the insensitivity of the catalyst to large excesses of typical poisons (see below) is not consistent with nanoparticle catalysis.

Kinetics and Mechanistic Experiments. Kinetic analysis of the rate of 1-hexene isomerization reveals a first-order dependency for 1-hexene. The kinetic traces do not show induction periods, which is also consistent with a molecular catalyst. An Eyring analysis of the temperature dependent rate constants (30 °C − 60 °C) gives activation parameters $\Delta H^{‡}$ = 11.5 ± 0.5 kcal/mol and $\Delta S^{‡}$ = −31.5 ± 1.5 e.u. The magnitude of $\Delta S^{‡}$ is notable, suggesting a highly ordered transition state. These activation parameters give $\Delta G^{‡}$ = 21.6 ± 1.0 kcal/mol at 40 °C.

An isotope labeling experiment provides additional mechanistic insight. At 40 °C, the rate of 1-hexene-3,3-D_2[32] isomerization (k_{obs} = 2.97 × 10^{-5} s^{-1}) provides a kinetic isotope effect, k_H/k_D = 2.9. The KIE is temperature independent, and thus tunneling does not play a role in the reaction mechanism. The combined experimental results are most consistent with alkene isomerization by **2** occurring by the allyl mechanism, akin to many other low valent iron complexes.[33]

Importantly, neopentane is not observed during catalysis. In addition, no new deuterium-containing products are observed when the reaction of **2** with $D_2C{=}C(D)CD_3$ is monitored by ^{2}H NMR spectroscopy. Thus, products resulting from loss of the neopentyl ligand, e.g. $(H_3C)_3CCH_2D$ or $D_2C{=}C(D)CH_2C(CH_3)_3$ are not observed within the detection limits of the measurement. Together, these observations suggest that the neopentyl ligand remains bound to iron during catalysis.

Computational Investigation. While the experimental data are most consistent with the allyl mechanism for alkene isomerization, they do not provide insight into the role of spin states. Since the strength of the ligand field is expected to increase for η^3-allyl intermediates in the allyl mechanism, lower spin states may be catalytically relevant. We therefore used computational methods to better understand the isomerization mechanism, and particularly the involvement of other spin states. For computational expediency, these calculations were performed with 1-butene as the substrate; however, all other features of the experimental system were retained. It is also important to note that these calculations are calibrated to experimental measurements.[34] While several possible mechanisms were investigated,[34] only the allyl mechanism is consistent with experimental observations. The lowest energy computed cycle is shown in Scheme 2, with the reaction coordinate shown in Figure 3.

Scheme 2

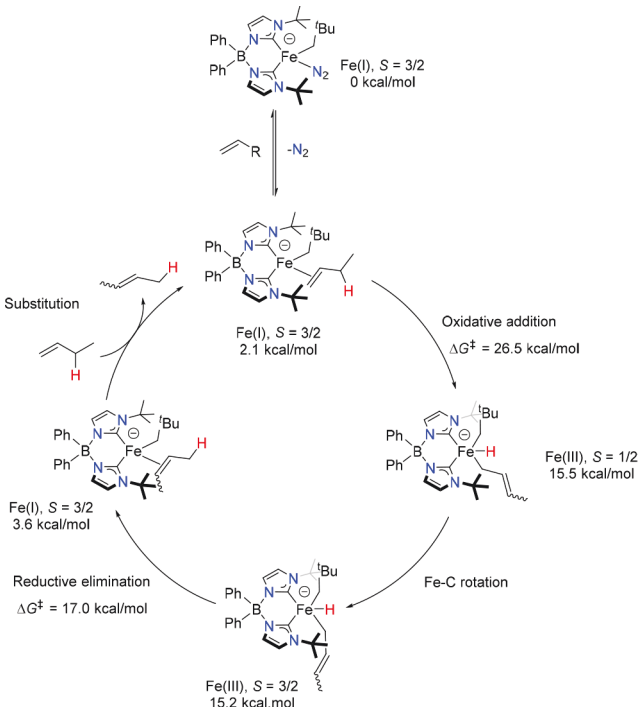

Substitution of the dinitrogen ligand by the alkene substrate provides entry into the catalytic cycle. This step is calculated to be modestly uphill thermodynamically (ΔG = 2.1 kcal/mol). The alkene can bind in one of two isoenergetic orientations, where the alkyl tail is either *syn* or *anti* to the diphenylborate group. Despite the stronger ligand field, the iron(I) η^2-alkene complex ^{4}**A** is calculated to have an S = 3/2 ground spin state. As described above, the crystallographically characterized η^2-alkyne complex **3** has a high spin (S = 3/2) ground state.

In accord with the allyl mechanism, oxidative addition of the allylic C−H bond provides an iron(III) allyl hydride complex. Here, the η^1-allyl isomers ^{2}**B** (S = 1/2) and ^{4}**B** (S = 3/2) are found to be 15.5 and 19.7 kcal/mol higher in energy than the dinitrogen complex **2**, respectively. Surprisingly, the η^3-allyl complex ^{2}**B′** (S = 1/2) is significantly higher in energy, making it unlikely to be mechanistically relevant. While we were unable to optimize the η^3-allyl complex on the S = 3/2 surface, this species is expected to be even higher in energy. The greater stability of the η^1-allyl intermediates is likely the result of destabilizing steric interactions in the η^3-allyl complex ^{2}**B′**, where the iron center is seven-coordinate.

A transition state for the oxidative addition step (^{2}**TS1**) was located on the S = 1/2 surface, with $\Delta G^{‡}$ = 26.5 kcal/mol. This is the highest energy species on the reaction surface, and the

https://dx.doi.org/10.1021/jacs.0c07300
J. Am. Chem. Soc. 2020, 142, 15527−15535

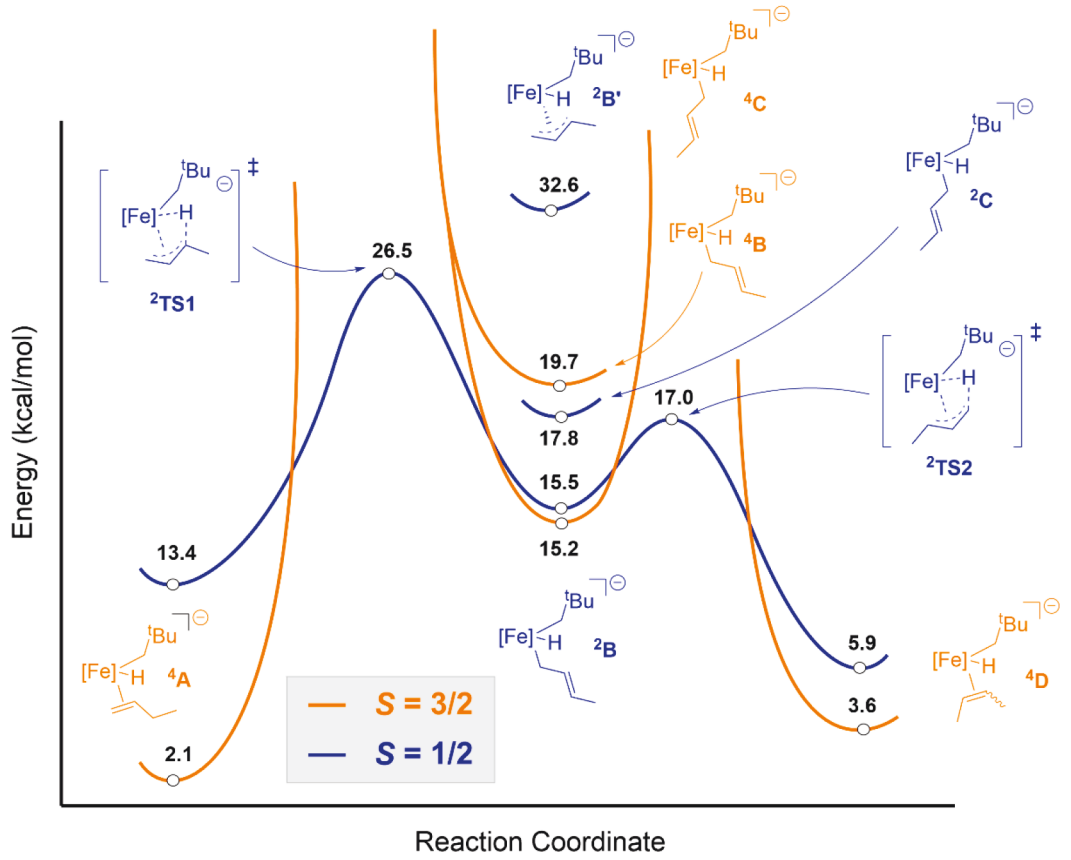

Figure 3. Calculated reaction coordinate for alkene isomerization by **2**. Relative energies in kcal/mol. Orange and blue curves represent $S = 3/2$ and $S = 1/2$ potential energy surfaces, respectively.

computed activation free energy is in good agreement with that determined experimentally, where $\Delta G^{\ddagger} = 21.6 \pm 1.0$ kcal/mol. Although an optimized transition state could not be located on the $S = 3/2$ surface, linear synchronous transit (LST) and quadratic synchronous transit (QST) analysis suggests the barrier is at least 15 kcal/mol higher in energy. The need for a spin state change can be understood by considering the orbital requirements for oxidative addition. Specifically, two electron oxidative addition requires an empty metal-based orbital to create the new iron-hydride bond. However, since all orbitals are at least partially occupied in the $S = 3/2$ spin state, this reaction is "spin blocked".[35]

The computed structure of ^{2}**TS1** is "η^3-allyl like" (Figure 4). Compared to ^{4}**A**, in ^{2}**TS1** there is an increase in the C1−C2 distance and a decrease in the C2−C3 distance, such that these bonds are of similar length, and intermediate between single and double bond lengths. In addition, the distances from iron to the carbon atoms of the allyl ligand are similar to those in structurally characterized iron η^3-allyl complexes.[36] This highly ordered transition state structure is in accord with the large magnitude of the experimentally determined entropy of activation, where $\Delta S^{\ddagger} = -31.5 \pm 1.5$ e.u. The allylic C−H bond is largely broken in ^{2}**TS1**, as characterized by the long C3−H distance (1.550 Å) and an Fe−H distance (1.540 Å) that is similar to paramagnetic iron hydride complexes.[37] These bond length changes are also consistent with the experimentally observed KIE, which shows that the rate depends on cleavage of the allylic C−H bond.

The next step of the reaction mechanism involves rotation about the Fe-allyl bond in ^{2}**B**. Here, the lowest energy structure

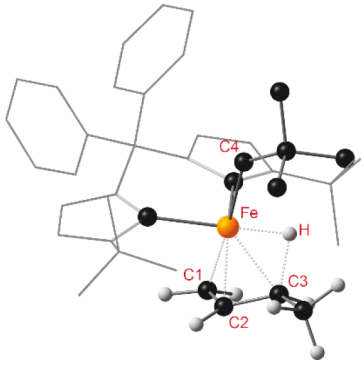

Figure 4. Computed transition state ^{2}**TS1**. Selected bond lengths (Å): Fe−H 1.541; Fe−C1 2.120; Fe−C2 1.975; Fe−C3 2.119; Fe−C4 2.141; C1−C2 1.427; C2−C3 1.442; C3−H 1.550.

is computed to be the $S = 3/2$ η^1-allyl intermediate ^{4}**C**, likely as a result of decreased steric interactions upon rotation. However, the small energy difference between the $S = 3/2$ (17.8 kcal/mol) and $S = 1/2$ (15.2 kcal/mol) surfaces suggests the states are highly mixed. Following bond rotation, reductive elimination provides ^{4}**D**, in which the alkene ligand has been isomerized. As with oxidative addition, reductive elimination is only viable on the $S = 1/2$ surface, with the transition state (^{2}**TS2**) also having an "η^3-allyl like" structure. The barrier to reductive elimination ($\Delta G^{\ddagger} = 17.0$ kcal/mol) is lower than that for oxidative addition, likely due to attenuated steric interactions in this step. The final step of the mechanism involves alkene ligand substitution to release the isomerized product, which is computed to be thermoneutral.

https://dx.doi.org/10.1021/jacs.0c07300
J. Am. Chem. Soc. 2020, 142, 15527−15535

In summary, the computationally determined mechanism is consistent with a reaction surface that traverses two spin states (i.e., two-state reactivity). Importantly, this mechanism is consistent with experimentally determined data, including the magnitudes of $\Delta G^{\ddagger}$ and $\Delta S^{\ddagger}$ as well as the observed kinetic isotope effect. An important insight from these studies is that $S = 1/2$ transition states are stabilized by the "η^3-allyl like" geometry of the alkene substrate.

The computational analysis also provides insight into the unexpected stability of the neopentyl ligand (see above). While reductive elimination of neopentane to provide $Ph_2B(^tBuIm)_2Fe(\eta^3\text{-allyl})$ ($S = 3/2$) from ^{2}**B** is calculated to be endergonic ($\Delta G = -14.2$ kcal/mol), the transition state is calculated to be thermally inaccessible ($\Delta G^{\ddagger} > 40$ kcal/mol). Indeed, an LST calculation reveals that the transition state for reductive elimination of neopentane is ~10 kcal/mol higher in energy than for the reductive elimination of the isomerized alkene. Since the orbital requirements for reductive elimination are the same as those of oxidative addition (see above), this reaction can only occur on the $S = 1/2$ surface. However, in contrast to reductive elimination of the alkene, an "η^3-allyl-like" transition state for the reductive elimination of neopentane is inaccessible. While the η^3-allyl complex ^{2}B′ provides another entry point to the $S = 1/2$ surface, this species is also thermally inaccessible. Finally, formation of neopentane requires C(sp^3)-H reductive elimination, which is less favorable than the C(sp^2)-H reductive elimination step leading to alkene isomerization. Therefore, although neopentane reductive elimination is thermodynamically favorable, kinetic barriers disfavor this process.

Binding Studies. A key aspect of the proposed reaction mechanism is that alkene binding only occurs on the $S = 3/2$ surface, whereas oxidative addition/reductive elimination only occurs on the $S = 1/2$ surface. Thus, the reaction steps are associated with distinct spin states, each with its own chemical properties. This presents an opportunity to harness two-state reactivity for selective catalysis.

Since all iron-based orbitals in the $S = 3/2$ state are at least partially occupied, we anticipate that neutral σ-donor ligands will only weakly bind to the metal. High d-electron counts have been shown to weaken the binding of additional ligands in low coordinate 3d metal complexes.[38] To provide support for this hypothesis, the binding abilities of a series of 4-substituted pyridines were evaluated according the equilibrium constant K_{eq}:[39]

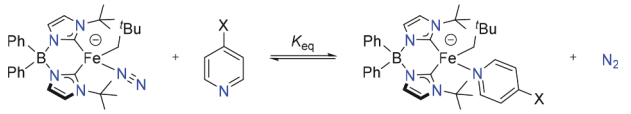

As demonstrated for the case of pyridine (X = H), significant changes are observed in the UV−vis spectrum when the base is titrated into a solution of **2** (Figure S28). These spectroscopic changes allow K_{eq} to be determined according to a weak binding model, providing $K_{eq} = (5.4 \pm 0.9) \times 10^{-4}$:

$$\frac{[2\text{–py}]}{[2]_0} = \frac{K_{eq}[\text{py}]_0}{K_{eq}[\text{py}]_0 + [\text{N}_2]} \quad (1)$$

where $[2]_0$ and $[\text{py}]_0$ are the initial concentrations of **2** of pyridine, respectively.[34] This study reveals that the binding of pyridine to **2** is significantly less favorable than N_2 binding.

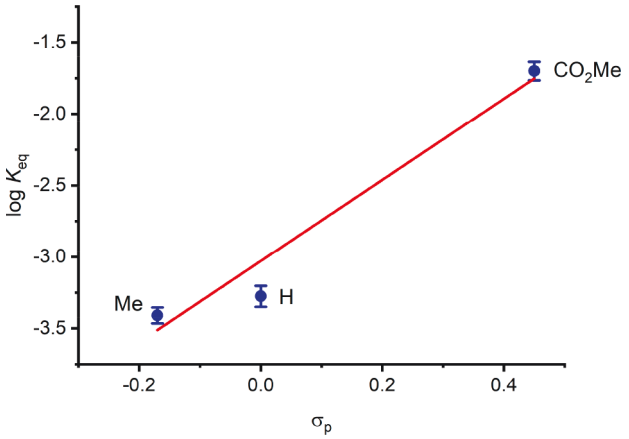

Figure 5. Hammett parameters of 4-substituted pyridines linearly correlate with the calculated log K_{eq} for **2** in THF.

There is a linear correlation between log K_{eq} and the Hammett parameter (σ_p)[40] for a series of 4-substituted pyridines. The positive slope ($\rho = +2.8$) indicates that electron-withdrawing groups facilitate binding to **2** (Figure 5),[41] counter to the typical expectations for ligand binding. Remarkably, there is no spectroscopic evidence that 4-dimethylaminopyridine (DMAP) binds to **2**, consistent with the Hammett plot (predicted $K_{eq} = 4.1 \times 10^{-6}$). This binding is not kinetically hindered, since reduction of the adduct between **1** and DMAP, which can be generated in situ from **1** and excess DMAP, provides **2** as the only iron-containing product.

A similar binding study for iron(II) complex **1** reveals a linear correlation between log (K_{eq}) and the Hammett parameter σ_{para} (Figure S26, $\rho = -2.0$). Thus, more basic σ-donor ligands bind more strongly to **1**, as expected from ligand field theory. Similar observations have been made for other low-coordinate transition metal complexes.[38,42]

The unusual ligand binding affinities of **2** can be rationalized by considering the electronic structure of the hypothetical three-coordinate, trigonal planar fragment $[Ph_2B(^tBuIm)_2FeCH_2{}^tBu]^-$, which is formed by loss of N_2 from **2**. Interactions between this metal fragment and the added base will determine the stability of the resultant complex. Notably, the SOMO − 1 is appropriately oriented for a favorable σ-symmetry interaction with an additional ligand (Figure 6a).

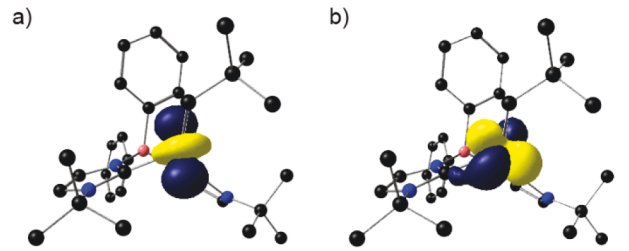

Figure 6. Selected frontier orbitals of the three-coordinate fragment $[Ph_2B(^tBuIm)_2FeCH_2{}^tBu]^-$. (a) SOMO − 1; (b) SOMO − 4.

However, since this orbital is half-filled, this interaction will necessarily be weak. Furthermore, the doubly occupied SOMO − 4 has the appropriate symmetry for interaction with a π-acidic ligand (Figure 6b), with the lobes of this orbital oriented such that the π-acidic ligand will occupy the apical position of the resulting trigonal pyramidal iron complex. This electronic

https://dx.doi.org/10.1021/jacs.0c07300
J. Am. Chem. Soc. 2020, 142, 15527−15535

structure is consistent with the geometry observed for complex **2**, where N_2 binds approximately perpendicularly to the trigonal plane about the iron center. The negative charge of $[Ph_2B(^tBuIm)_2FeCH_2{}^tBu]^-$ will enhance these weak σ-acid and good π-base properties by increasing the orbital energies on the complex. In addition, the negative charge will serve to electrostatically repel incoming bases, further decreasing the ligand binding affinities.

Alkene Isomerization in the Presence of σ-Bases. The poor affinity for σ-bases suggests that **2** will be catalytically active toward alkene isomerization in the presence of σ-basic ligands. Gratifyingly, high conversions to 2-hexene are observed in the presence of excess triethylamine, *N*-methylpyrrole, 4-*tert*-butylpyridine and pyridine,[43] bases that are often catalyst poisons.[44] Some bases (e.g., butyronitrile, methylimidazole, and 4-CF_3-pyridine) are observed to inhibit, although not completely shut down catalysis.[45] Of the bases investigated, only 4-methylthiazole completely inhibits isomerization (Table S2).

The ability of **2** to catalyze alkene isomerization in the presence of excess base was further investigated with DMAP, whose strong σ-donor abilities have been shown to inhibit other homogeneous catalysts. Remarkably, there is no change in the first-order rate constant (k_{obs}) for the isomerization of 1-hexene to 2-hexene in the presence of up to 0.75 M DMAP (Figure 7).

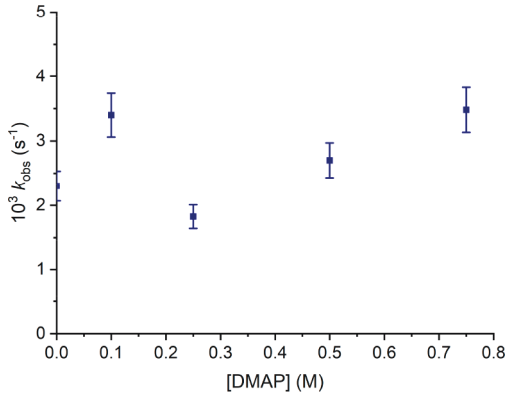

Figure 7. Catalytic isomerization of 1-hexene by **2** in the presence of excess DMAP. No change in the first-order rate constant is observed. Initial conditions: [2] = 50 mM; [1-hexene] = 0.5 M in THF-d_8.

CONCLUSIONS

A combined experimental and computational investigation of the mechanism of alkene isomerization by the high spin (S = 3/2) iron(I) complex **2** is most consistent with the reaction occurring by the allyl pathway. These studies reveal that alkene binding occurs on the S = 3/2 surface, whereas the transition states that lead to alkene isomerization are on the S = 1/2 surface. Due to the high spin configuration, the binding of σ-bases on the S = 3/2 surface is generally weak, and consequently **2** has good immunity to these typical catalyst poisons.

While binding of the alkene substrate is likely enhanced by the π-basic properties of **2**, we anticipate that the concepts described in this work can be extended to other catalytic processes. Thus, transition-metal catalyzed reactions in which substrate binding enables two-state reactivity may allow for selectivity based on the reactivity properties of the two spin states. Catalytic reactions that involve "spin acceleration" are expected to be the most favorable in this regard due to the different spin states of the reaction intermediates and reaction transition states.

ASSOCIATED CONTENT

Supporting Information

The Supporting Information is available free of charge at https://pubs.acs.org/doi/10.1021/jacs.0c07300.

Full experimental procedures, computational details, and crystallographic information (PDF)

Coordinates of optimized structures (XYZ)

CCDC 2014746-2014748 contains the supplementary crystallographic data for this paper, which can be obtained free of charge from The Cambridge Crystallographic Data Centre via www.ccdc.cam.ac.uk/structures (CIF)

AUTHOR INFORMATION

Corresponding Author

Jeremy M. Smith − *Department of Chemistry, Indiana University, Bloomington, Indiana 47405, United States;* orcid.org/0000-0002-3206-4725; Email: smith962@indiana.edu

Authors

Sean A. Lutz − *Department of Chemistry, Indiana University, Bloomington, Indiana 47405, United States*

Anne K. Hickey − *Department of Chemistry, Indiana University, Bloomington, Indiana 47405, United States*

Yafei Gao − *Department of Chemistry, Indiana University, Bloomington, Indiana 47405, United States;* orcid.org/0000-0001-7970-8535

Chun-Hsing Chen − *Department of Chemistry, Indiana University, Bloomington, Indiana 47405, United States;* orcid.org/0000-0003-0150-9557

Complete contact information is available at: https://pubs.acs.org/10.1021/jacs.0c07300

Author Contributions

†S.A.L., A.K.H., and Y.G. contributed equally.

Notes

The authors declare no competing financial interest.

ACKNOWLEDGMENTS

This material is based upon work supported by the U.S. Department of Energy, Office of Science, Office of Basic Energy Sciences Energy Frontier Research Centers program under Award Number DE-SC-0019466. Funding from IU and the NSF (CHE-1112299 and CHE-1566258) is also acknowledged.

REFERENCES

(1) (a) Plietker, B. *Iron Catalysis in Organic Chemistry: Reactions and Applications*; Wiley-VCH: New York, 2008. (b) Plietker, B. *Iron Catalysis. Fundamentals and Applications*; Springer International Publishing: Switzerland, 2011. (c) Bauer, E. *Iron Catalysis II*; Springer International Publishing: Switzerland, 2015.

(2) Selected reviews: (a) Bauer, I.; Knölker, H.-J. Iron Catalysis in Organic Synthesis. *Chem. Rev.* **2015**, *115*, 3170−3387. (b) Wei, D.; Darcel, C. Iron Catalysis in Reduction and Hydrometalation Reactions. *Chem. Rev.* **2019**, *119*, 2550−2610.

(3) (a) Chirik, P. J.; Wieghardt, K. Radical Ligands Confer Nobility on Base-Metal Catalysts. *Science* **2010**, *327*, 794−795. (b) Fürstner, A. Iron Catalysis in Organic Synthesis: A Critical Assessment of What It Takes To Make This Base Metal a Multitasking Champion. *ACS Cent. Sci.* **2016**, *2*, 778−789. (c) Arevalo, R.; Chirik, P. J. Enabling Two-Electron

Pathways with Iron and Cobalt: From Ligand Design to Catalytic Applications. *J. Am. Chem. Soc.* **2019**, *141*, 9106−9123.
(4) Selected reviews: (a) Schröder, D.; Shaik, S.; Schwarz, H. Two-State Reactivity as a New Concept in Organometallic Chemistry. *Acc. Chem. Res.* **2000**, *33*, 139−145. (b) Dzik, W. I.; Böhmer, W.; de Bruin, B. Multiple Spin-State Scenarios in Organometallic Reactivity. In *Spin States in Biochemistry and Inorganic Chemistry: Influence on Structure and Reactivity*; Swart, M., Costas, M., Eds.; John Wiley & Sons: Chichester, 2016.
(5) (a) Shaik, S.; Hirao, H.; Kumar, D. Reactivity of High-Valent Iron−Oxo Species in Enzymes and Synthetic Reagents: A Tale of Many States. *Acc. Chem. Res.* **2007**, *40*, 532−542. (b) Shaik, S.; Kumar, D.; de Visser, S. P.; Altun, A.; Thiel, W. Theoretical Perspective on the Structure and Mechanism of Cytochrome P450 Enzymes. *Chem. Rev.* **2005**, *105*, 2279−2328. (c) Shaik, S.; Cohen, S.; Wang, Y.; Chen, H.; Kumar, D.; Thiel, W. P450 Enzymes: Their Structure, Reactivity, and Selectivity - Modeled by QM/MM Calculations. *Chem. Rev.* **2010**, *110*, 949−1017.
(6) Leadbeater, N. Enlightening Organometallic Chemistry: The Photochemistry of $Fe(CO)_5$ and the Reaction Chemistry of Unsaturated Iron Carbonyl Fragments. *Coord. Chem. Rev.* **1999**, *188*, 35−70.
(7) (a) Besora, M.; Carreón-Macedo, J.-L.; Cowan, A. J.; George, M. W.; Harvey, J. N.; Portius, P.; Ronayne, K. L.; Sun, X.-Z.; Towrie, M. A Combined Theoretical and Experimental Study on the Role of Spin States in the Chemistry of $Fe(CO)_5$ Photoproducts. *J. Am. Chem. Soc.* **2009**, *131*, 3583−3592. (b) Besora, M.; Carreón-Macedo, J.-L.; Cimas, A.; Harvey, J. N. Spin-State Changes and Reactivity in Transition Metal Chemistry: Reactivity of Iron Tetracarbonyl. *Adv. Inorg. Chem.* **2009**, *61*, 573−623.
(8) (a) Bellows, S. M.; Cundari, T. R.; Holland, P. L. Spin Crossover during β-Hydride Elimination in High-Spin Iron(II)− and Cobalt(II)−Alkyl Complexes. *Organometallics* **2013**, *32*, 4741−4751. (b) Takayanagi, T.; Saito, K.; Suzuki, H.; Watabe, Y.; Fujihara, T. Computational Analysis of Two-State Reactivity in β-Hydride Elimination Mechanisms of Fe(II)− and Co(II)−Alkyl Complexes Supported by β-Diketiminate Ligand. *Organometallics* **2019**, *38*, 3582−3589.
(9) (a) Baker, M. V.; Field, L. D. Reaction of sp^2 C-H bonds in Unactivated Alkenes with Bis(diphosphine) Complexes of Iron. *J. Am. Chem. Soc.* **1986**, *108*, 7433−7434. (b) Jones, W. D.; Foster, G. P.; Putinas, J. M. The Catalytic Activation and Functionalization of C-H Bonds. Aldimine Formation by the Insertion of Isonitriles into Aromatic C-H Bonds. *J. Am. Chem. Soc.* **1987**, *109*, 5047−5048. (c) Macgregor, S. A.; Eisenstein, O.; Whittlesey, M. K.; Perutz, R. N. A Theoretical Study of $[M(PH_3)_4]$ (M = Ru or Fe), Models for the Highly Reactive d^8 Intermediates $[M(dmpe)_2]$ (dmpe = $Me_2PCH_2CH_2PMe_2$). Zero Activation Energies for Addition of CO and Oxidative Addition of H_2. *J. Chem. Soc., Dalton Trans.* **1998**, 291−300. (d) Harvey, J. N.; Poli, R. Computational Study of the Spin-Forbidden H_2 Oxidative Addition to 16-Electron Fe(0) Complexes. *Dalton Trans.* **2003**, 4100−4106. (e) Hickey, A. K.; Lutz, S. A.; Chen, C.-H.; Smith, J. M. Two-State Reactivity in C−H Activation by a Four-Coordinate Iron(0) Complex. *Chem. Commun.* **2017**, *53*, 1245−1248.
(10) (a) Kalman, S. E.; Petit, A.; Gunnoe, T. B.; Ess, D. H.; Cundari, T. R.; Sabat, M. Facile and Regioselective C−H Bond Activation of Aromatic Substrates by an Fe(II) Complex Involving a Spin-Forbidden Pathway. *Organometallics* **2013**, *32*, 1797−1806. (b) Sun, Y.; Tang, H.; Chen, K.; Hu, L.; Yao, J.; Shaik, S.; Chen, H. Two-State Reactivity in Low-Valent Iron-Mediated C−H Activation and the Implications for Other First-Row Transition Metals. *J. Am. Chem. Soc.* **2016**, *138*, 3715−3730.
(11) Holland, P. L. Distinctive Reaction Pathways at Base Metals in High-Spin Organometallic Catalysts. *Acc. Chem. Res.* **2015**, *48*, 1696−1702.
(12) (a) Yang, J.; Tilley, T. D. Efficient Hydrosilylation of Carbonyl Compounds with the Simple Amide Catalyst $[Fe\{N(SiMe_3)_2\}_2]$. *Angew. Chem., Int. Ed.* **2010**, *49*, 10186−10188. (b) Fan, G.; Shang, Z.; Li, R.; Shafiei-Haghighi, S.; Peng, Q.; Findlater, M.; Xu, X. Mechanism of the Iron(0)-Catalyzed Hydrosilylation of Aldehydes: A Combined DFT and Experimental Investigation. *Organometallics* **2019**, *38*, 4105−4114.
(13) Macaulay, C. M.; Gustafson, S. J.; Fuller, J. T., III; Kwon, D.-H.; Ogawa, T.; Ferguson, M. J.; McDonald, R.; Lumsden, M. D.; Bischof, S. M.; Sydora, O. L.; Ess, D. H.; Stradiotto, M.; Turculet, L. Alkene Isomerization−Hydroboration Catalyzed by First-Row Transition-Metal (Mn, Fe, Co, and Ni) N-Phosphinoamidinate Complexes: Origin of Reactivity and Selectivity. *ACS Catal.* **2018**, *8*, 9907−9925.
(14) Hu, L.; Chen, H. Substrate-Dependent Two-State Reactivity in Iron-Catalyzed Alkene [2 + 2] Cycloaddition Reactions. *J. Am. Chem. Soc.* **2017**, *139*, 15564−15567.
(15) Hedström, A.; Lindstedt, E.; Norrby, P.-O. Ox the Oxidation State of Iron in Iron-Mediated C-C Couplings. *J. Organomet. Chem.* **2013**, *748*, 51−55.
(16) Fisher, M. T.; Sligar, S. G. Control of Heme Protein Redox Potential and Reduction Rate: Linear Free Energy Relation between Potential and Ferric Spin State Equilibrium. *J. Am. Chem. Soc.* **1985**, *107*, 5018−5019.
(17) (a) Turner, J. W.; Schultz, F. A. Coupled Electron-Transfer and Spin-Exchange Reactions. *Coord. Chem. Rev.* **2001**, *219*−*221*, 81−97. (b) Schultz, F. A. Structure-Reactivity Relationships in Inorganic Electrochemistry. *J. Solid State Electrochem.* **2011**, *15*, 1833−1843.
(18) Hickey, A. K.; Lee, W.-T.; Chen, C.-H.; Pink, M.; Smith, J. M. A Bidentate Ligand Stabilizes a Low-Coordinate Iron(0) Carbonyl Complex. *Organometallics* **2016**, *35*, 3069−3073.
(19) For example: (a) Fernández, I.; Trovitch, R. J.; Lobkovsky, E.; Chirik, P. J. Synthesis of Bis(imino)pyridine Iron Di- and Monoalkyl Complexes: Stability Differences between $FeCH_2SiMe_3$ and $FeCH_2CMe_3$ Derivatives. *Organometallics* **2008**, *27*, 109−118. (b) Vela, J.; Cirera, J.; Smith, J. M.; Lachicotte, R. J.; Flaschenriem, C. J.; Alvarez, S.; Holland, P. L. Quantitative Geometric Descriptions of the Belt Iron Atoms of the Iron−Molybdenum Cofactor of Nitrogenase and Synthetic Iron(II) Model Complexes. *Inorg. Chem.* **2007**, *46*, 60−71.
(20) (a) Andres, H.; Bominaar, E. L.; Smith, J. M.; Eckert, N. A.; Holland, P. L.; Münck, E. Planar Three-Coordinate High-Spin FeII Complexes with Large Orbital Angular Momentum: Mössbauer, Electron Paramagnetic Resonance, and Electronic Structure Studies. *J. Am. Chem. Soc.* **2002**, *124*, 3012−3025. (b) Cowley, R. E.; Bill, E.; Neese, F.; Brennessel, W. W.; Holland, P. L. Iron(II) Complexes with Redox-Active Tetrazene (RNNNNR) Ligands. *Inorg. Chem.* **2009**, *48*, 4828−4836. (c) Dugan, T. R.; Bill, E.; MacLeod, K. C.; Brennessel, W. W.; Holland, P. L. Synthesis, Spectroscopy, and Hydrogen/Deuterium Exchange in High-Spin Iron(II) Hydride Complexes. *Inorg. Chem.* **2014**, *53*, 2370−2380.
(21) Liu, Y.; Wang, L.; Deng, L. Three-Coordinate Iron(II) Dialkenyl Compound with NHC Ligation: Synthesis, Structure, and Reactivity. *Organometallics* **2015**, *34*, 4401−4407.
(22) In the absence of cryptand, the complex $\{[K][Ph_2B(^tBuIm)_2FeCH_2{}^tBu(N_2)]\}_2(THF)_4$ is formed, demonstrating that cryptand is not essential for N_2 coordination (ν_{NN} = 1877 cm^{-1}, KBr). However, since this complex can only be isolated in only poor yield, complex **2** is more practical for use in catalysis.
(23) (a) Tondreau, A. M.; Milsmann, C.; Patrick, A. D.; Hoyt, H. M.; Lobkovsky, E.; Wieghardt, K.; Chirik, P. J. Synthesis and Electronic Structure of Cationic, Neutral, and Anionic Bis(imino)pyridine Iron Alkyl Complexes: Evaluation of Redox Activity in Single-Component Ethylene Polymerization Catalysts. *J. Am. Chem. Soc.* **2010**, *132*, 15046−15059. (b) Kuriyama, S.; Arashiba, K.; Nakajima, K.; Matsuo, Y.; Tanaka, H.; Ishii, K.; Yoshizawa, K.; Nishibayashi, Y. Catalytic Transformation of Dinitrogen into Ammonia and Hydrazine by Iron-Dinitrogen Complexes Bearing Pincer Ligand. *Nat. Commun.* **2016**, *7*, 12181. (c) Ouyang, Z.; Cheng, J.; Li, L.; Bao, X.; Deng, L. High-Spin Iron(I) and Iron(0) Dinitrogen Complexes Supported by N-Heterocyclic Carbene Ligands. *Chem. - Eur. J.* **2016**, *22*, 14162−14165. (d) Fan, Y.; Cheng, J.; Gao, Y.; Shi, M.; Deng, L. Iron Dinitrogen Complexes Supported by Tris(NHC)borate Ligand: Synthesis, Characterization, and Reactivity Study. *Huaxue Xuebao* **2018**, *76*, 445−452.

https://dx.doi.org/10.1021/jacs.0c07300
J. Am. Chem. Soc. 2020, 142, 15527−15535

(24) Blume, M. Magnetic Relaxation and Asymmetric Quadrupole Doublets in the Mössbauer Effect. *Phys. Rev. Lett.* **1965**, *14*, 96−98.
(25) Davydov, R. M.; McLaughlin, M. P.; Bill, E.; Hoffman, B. M.; Holland, P. L. Generation of High-Spin Iron(I) in a Protein Environment Using Cryoreduction. *Inorg. Chem.* **2013**, *52*, 7323−732.
(26) Chiang, K. P.; Scarborough, C. C.; Horitani, M.; Lees, N. S.; Ding, K.; Dugan, T. R.; Brennessel, W. W.; Bill, E.; Hoffman, B. M.; Holland, P. L. Characterization of the Fe-H bond in a Three-Coordinate Terminal Hydride Complex of Iron(I). *Angew. Chem., Int. Ed.* **2012**, *51*, 3658−3662.
(27) Yu, Y.; Smith, J. M.; Flaschenriem, C. J.; Holland, P. L. Binding Affinity of Alkynes and Alkenes to Low-Coordinate Iron. *Inorg. Chem.* **2006**, *45*, 5742−5751.
(28) Ye, S.; Bill, E.; Neese, F. Electronic Structures of the $[Fe(N_2)(SiP^iPr_3)]^{+1/0/-1}$ Electron Transfer Series: A Counterintuitive Correlation between Isomer Shifts and Oxidation States. *Inorg. Chem.* **2016**, *55*, 3468−3474.
(29) The *trans*:*cis* ratio was determined from the integrations of the ^{13}C resonances at the olefin chemical shifts for *cis*- and *trans*-2-hexene. See the SI (Figure S20) for details.
(30) Phua, P.-H.; Lefort, L.; Boogers, J. A. F.; Tristany, M.; de Vries, J. G. Soluble Iron Nanoparticles as Cheap and Environmentally Benign Alene and Alkyne Hydrogenation Catalysts. *Chem. Commun.* **2009**, 3747−3749.
(31) (a) Mørup, S.; Linderoth, S.; Jacobsen, J.; Holmblad, M. Temperature Dependence of the Magnetic Hyperfine Splitting of Metastable Iron-Amalgam. *Hyperfine Interact.* **1992**, *69*, 489−492. (b) Linderoth, S.; Mørup, S. Stability and Magnetic Properties of an Iron-Mercury Alloy. *J. Phys.: Condens. Matter* **1992**, *4*, 8627−8634.
(32) Sirokan, G.; Molnar, A.; Bartok, M. Synthesis of Deuterium-Labelled Alkenes. *J. Labelled Compd. Radiopharm.* **1989**, *27*, 439−448.
(33) (a) Schroeder, M. A.; Wrighton, M. A. Pentacarbonyliron(0) Photocatalyzed Hydrogenation and Isomerization of Olefins. *J. Am. Chem. Soc.* **1976**, *98*, 551−558. (b) Mitchener, J. C.; Wrighton, M. A. Photogeneration of Very Active Homogeneous Catalysts Using Laser Light Excitation of Iron Carbonyl Precursors. *J. Am. Chem. Soc.* **1981**, *103*, 975−977. (c) Perthuisot, C.; Jones, W. D. C-H Activation of Olefins with a Zerovalent Iron Complex − Isomerization of 4-Phenyl-1-butene to 1-Phenyl-1-butene using $Fe(depe)_2N_2$. *New J. Chem.* **1994**, *18*, 621−628. (d) Glascoe, E. A.; Sawyer, K. R.; Shanoski, J. E.; Harris, C. B. The Influence of the Metal Spin State in the Iron-Catalyzed Alkene Isomerization Reaction Studied with Ultrafast Infrared Spectroscopy. *J. Phys. Chem. C* **2007**, *111*, 8789−8795. (e) Sawyer, K. R.; Glascoe, E. A.; Cahoon, J. F.; Schlegel, J. P.; Harris, C. B. Mechanism for Iron-Catalyzed Alkene Isomerization in Solution. *Organometallics* **2008**, *27*, 4370−4379. (f) Furstner, A.; Majima, K.; Martin, R.; Krause, H.; Kattnig, E.; Goddard, R.; Lehmann, C. W. A Cheap Metal for a "Noble" Task: Preparative and Mechanistic Aspects of Cycloisomerization and Cycloaddition Reactions Catalyzed by Low-Valent Iron Complexes. *J. Am. Chem. Soc.* **2008**, *130*, 1992−2004. (g) Mayer, M.; Welther, A.; Jacobi von Wangelin, A. Iron-Catalyzed Isomerizations of Olefins. *ChemCatChem* **2011**, *3*, 1567−1571. (h) Russell, S. K.; Lobkovsky, E.; Chirik, P. J. Iron-Catalyzed Intermolecular $[2\pi + 2\pi]$ Cycloaddition. *J. Am. Chem. Soc.* **2011**, *133*, 8858−8861. (i) Liu, X.; Li, B.; Liu, Q. Base-Metal-Catalyzed Olefin Isomerization Reactions. *Synthesis* **2019**, *51*, 1293−1310.
(34) See the SI for full details.
(35) Selected examples: (a) Keogh, D. W.; Poli, R. Spin State Change in Organometallic Reactions. Experimental and MP2 Theoretical Studies of the Thermodynamics and Kinetics of the CO and N_2 Addition to Spin Triplet $Cp^*MoCl(PMe_3)_2$. *J. Am. Chem. Soc.* **1997**, *119*, 2516−2523. (b) Carreón-Macedo, J.-L.; Harvey, J. N. Do Spin State Changes Matter in Organometallic Chemistry? A Computational Study. *J. Am. Chem. Soc.* **2004**, *126*, 5789−5797. (c) Hardman, N. J.; Fang, X.; Scott, B. L.; Wright, R. J.; Martin, R. L.; Kubas, G. J. High-Spin Diimine Complexes of Iron(II) Reject Binding of Carbon Monoxide: Theoretical Analysis of Thermodynamic Factors Inhibiting or Favoring Spin-Crossover. *Inorg. Chem.* **2005**, *44*, 8306−8316. (d) Benito-Garagorri, D.; Alves, L. G.; Veiros, L. F.; Standfest-Hauser, C. M.; Tanaka, S.; Mereiter, K.; Kirchner, K. Kinetically Controlled Formation of Octahedral trans-Dicarbonyl Iron(II) PNP Pincer Complexes: The Decisive Role of Spin-State Changes. *Organometallics* **2010**, *29*, 4932−4942. (e) Watanabe, K.; Nakatani, N.; Nakayama, A.; Higashi, M.; Hasegawa, J. Spin-Blocking Effect in CO and H_2 Binding Reactions to Molybdenocene and Tungstenocene: A Theoretical Study on the Reaction Mechanism via the Minimum Energy Intersystem Crossing Point. *Inorg. Chem.* **2016**, *55*, 8082−8090.
(36) (a) Simon, F. E.; Lauher, J. W. Synthesis and Molecular Structure of $(\eta^3\text{-}C_3H_5)Fe(CO)_3AuP(C_6H_5)_3$ and the Molecular Structure of $(\eta^3\text{-}C_3H_5)Fe(CO)_3Br$. Two Compounds with Distinctly Different Coordination Geometries. *Inorg. Chem.* **1980**, *19*, 2338−2343. (b) Brunner, H.; Weber, H.; Bernal, I.; Reisner, G. M. Optically Active Transition-Metal Compounds. 80. Synthesis, Stereochemistry, and X-ray Analysis of Allylcarbonylnitrosyl(aminophosphine)iron Complexes. *Organometallics* **1984**, *3*, 163−170. (c) Yu, Y.-F; Gallucci, J.; Wojcicki, A. New Bimetallic, Phosphido-Bridged Iron Complexes Derived from $[Fe_2(\mu\text{-}CO)(\mu\text{-}PPh_2)(CO)_5(PPh_2)]^{2-}$. *J. Chem. Soc., Chem. Commun.* **1984**, 653−655. (d) Nakanishi, S.; Memita, S.; Takata, T.; Itoh, K. Preparation, Ligand Substitution, and Structural Stability of $(\eta^3$-Allyl)dicarbonylnitrosyliron Complexes. *Bull. Chem. Soc. Jpn.* **1998**, *71*, 403−412. (e) Trovitch, R. J.; Lobkovsky, E.; Bouwkamp, M. W.; Chirik, P. J. Carbon−Oxygen Bond Cleavage by Bis(imino)pyridine Iron Compounds: Catalyst Deactivation Pathways and Observation of Acyl C−O Bond Cleavage in Esters. *Organometallics* **2008**, *27*, 6264−6278. (f) Fürstner, A.; Martin, R.; Krause, H.; Seidel, G.; Goddard, R.; Lehmann, C. W. Preparation, Structure, and Reactivity of Nonstabilized Organoiron Compounds. Implications for Iron-Catalyzed Cross Coupling Reactions. *J. Am. Chem. Soc.* **2008**, *130*, 8773−8787.
(37) (a) Hamon, P.; Toupet, L.; Hamon, J. R.; Lapinte, C. Novel Diamagnetic and Paramagnetic Iron(II), Iron(III), and Iron(IV) Classical and Nonclassical Hydrides. X-ray Crystal Structure of $[Fe(C_5Me_5)(dppe)D]PF_6$. *Organometallics* **1992**, *11*, 1429−1431. (b) Chiang, K. P.; Scarborough, C. C.; Horitani, M.; Lees, N. S.; Ding, K.; Dugan, T. R.; Brennessel, W. W.; Bill, E.; Hoffman, B. M.; Holland, P. L. Characterization of the Fe−H Bond in a Three-Coordinate Terminal Hydride Complex of Iron(I). *Angew. Chem., Int. Ed.* **2012**, *51*, 3658−3662. (c) Gu, N. X.; Oyala, P. H.; Peters, J. C. An $S = 1/2$ Iron Complex Featuring N_2, Thiolate, and Hydride Ligands: Reductive Elimination of H_2 and Relevant Thermochemical Fe−H Parameters. *J. Am. Chem. Soc.* **2018**, *140*, 6374−6382.
(38) Lin, C.-Y.; Fettinger, J. C.; Power, P. P. Reversible Complexation of Lewis Bases to Low-Coordinate Fe(II), Co(II), and Ni(II) Amides: Influence of the Metal, Donor Ligand, and Amide Substituent on Binding Constants. *Inorg. Chem.* **2017**, *56*, 9892−9902.
(39) Connors, K. A. *Binding Constants: The Measurement of Molecular Complex Stability*; John Wiley & Sons: New York, 1987.
(40) Hansch, C.; Leo, A.; Taft, R. W. A Survey of Hammett Substituent Constants and Resonance and Field Parameters. *Chem. Rev.* **1991**, *91*, 165−196.
(41) (a) Mahapatra, S.; Halfen, J. A.; Tolman, W. B. Mechanistic Study of the Oxidative N-Dealkylation Reactions of Bis(μ-oxo)-dicopper Complexes. *J. Am. Chem. Soc.* **1996**, *118*, 11575−11586. (b) Johnson, C. D. *The Hammett Equation*; Cambridge University Press: Cambridge, UK, 1973.
(42) Chiang, K. P.; Barrett, P. M.; Ding, F.; Smith, J. M.; Kingsley, S.; Brennessel, W. W.; Clark, M. M.; Lachicotte, R. J.; Holland, P. L. Ligand Dependence of Binding to Three-Coordinate Fe(II) Complexes. *Inorg. Chem.* **2009**, *48*, 5106−5116.
(43) The choice of σ-bases was generally informed by those used for catalyst robustness screens, see (a) Collins, K. D.; Glorius, F. A Robustness Screen for the Rapid Assessment of Chemical Reactions. *Nat. Chem.* **2013**, *5*, 597−601. (b) Collins, K. D.; Glorius, F. Intermolecular Reaction Screening as a Tool for Reaction Evaluation. *Acc. Chem. Res.* **2015**, *48*, 619−627.
(44) Crabtree, R. H. Deactivation in Homogeneous Transition Metal Catalysis: Causes, Avoidance, and Cure. *Chem. Rev.* **2015**, *115*, 127−150.

https://dx.doi.org/10.1021/jacs.0c07300
J. Am. Chem. Soc. 2020, 142, 15527−15535

(45) The calculated redox potentials suggest that electron transfer could be a competitive reaction pathway for some of these bases, e.g. Dugan, T. R.; Bill, E.; MacLeod, K. C.; Christian, G. J.; Cowley, R. E.; Brennessel, W. W.; Ye, S.; Neese, F.; Holland, P. L. Reversible C−C Bond Formation between Redox-Active Pyridine Ligands in Iron Complexes. *J. Am. Chem. Soc.* **2012**, *134*, 20352−20364. See the SI (Table S2) for details.

https://dx.doi.org/10.1021/jacs.0c07300
J. Am. Chem. Soc. 2020, 142, 15527−15535